Effect of orientational restriction on monolayers of hard ellipsoids

Szabolcs Varga,[f] Yuri Martínez-Ratón,[a] Enrique Velasco,[b]
Gustavo Bautista-Carbajal[cd] and Gerardo Odriozola*[e]

The effect of out-of-plane orientational freedom on the orientational ordering properties of a monolayer of hard ellipsoids is studied using the Parsons–Lee scaling approach and replica exchange Monte Carlo computer simulation. Prolate and oblate ellipsoids exhibit very different ordering properties, namely, the axes of revolution of prolate particles tend to lean out, while those of oblate ones prefer to lean into the confining plane. The driving mechanism of this is that the particles try to maximize the available free area on the confining surface, which can be achieved by minimizing the cross section areas of the particles with the plane. In the lack of out-of-plane orientational freedom the monolayer of prolate particles is identical to a two-dimensional hard ellipse system, which undergoes an isotropic–nematic ordering transition with increasing density. With gradually switching on the out-of-plane orientational freedom the prolate particles lean out from the confining plane and destabilisation of the in-plane isotropic–nematic phase transition is observed. The system of oblate particles behaves oppositely to that of prolates. It corresponds to a two-dimensional system of hard disks in the lack of out-of-plane freedom, while it behaves similar to that of hard ellipses in the freely rotating case. Solid phases can be realised by lower surface coverage due to the out-of-plane orientation freedom for both oblate and prolate shapes.

1 Introduction

Phase behavior of non-spherical hard bodies with their centers of mass confined in planar geometry is receiving considerable attention due to the recent development of the preparation of colloidal particles with various shapes and new experimental techniques. Nowadays it is possible to prepare colloids with several geometrical shapes such as cubes, polyhedrons, octopods, ellipsoids and helices.[1–6] The anisotropic colloids can be confined at the interfaces,[7–11] between two parallel solid walls,[12,13] at the bottom of the sample holder,[14] at a substrate surface[15]

and into a lamellar matrix of surfactants.[16,17] The confinement can be so strong that even colloidal monolayers can be realized experimentally.

Ordering properties of two-dimensional and quasi two-dimensional (q2D) non-spherical colloids has been the subject of several experimental and theoretical studies.[17–36] The reason for this is that the nature of two-dimensional (2D) nematic ordering is quite different from the three-dimensional (3D) one. It shows only a quasi-long-range orientational order with algebraically decaying orientational correlations and the ordering transitions between isotropic and nematic phases are first order or continuous through a Kosterlitz–Thouless disclination unbinding type mechanism.[18,37]

Strictly 2D colloidal systems cannot be examined experimentally, because the out-of-plane orientational and positional freedoms are always present to some extent. Therefore it is desirable to extend the theoretical studies in such directions, where the extra orientational and positional freedoms are present. Along this line, the ordering properties of microtubules confined in a thin slit have been modeled as hard spherocylinders placed between two planar walls in ref. 28. In agreement with the experiment it has been found that the isotropic–nematic transition density increases with the wall separation.[28]

Ellipsoidal shaped colloidal particles are gaining widespread applications due to the development of the stretching techniques

[a] Grupo Interdisciplinar de Sistemas Complejos (GISC), Departamento de Matemáticas, Escuela Politécnica Superior, Universidad Carlos III de Madrid, Avenida de la Universidad 30, E-28911, Leganés, Madrid, Spain

[b] Departamento de Física Teórica de la Materia Condensada and Instituto de Ciencia de Materiales Nicolás Cabrera, Universidad Autónoma de Madrid, E-28049 Madrid, Spain

[c] Departamento de Física, Universidad Autónoma Metropolitana-Iztapalapa, 09340, México, Distrito Federal, Mexico

[d] Academia de Matemáticas, Universidad Autónoma de la Ciudad de México, 07160, México, D. F., Mexico

[e] Area de Física de Procesos Irreversibles, División de Ciencias Básicas e Ingeniería, Universidad Autónoma Metropolitana-Azcapotzalco, Av. San Pablo 180, 02200 México, D. F., Mexico. E-mail: godriozo@azc.uam.mx

[f] Institute of Physics and Mechatronics, University of Pannonia, PO Box 158, Veszprém, H-8201 Hungary

in the preparation of monodisperse prolate and oblate ellipsoids from spherical latex particles.[4,38] They can also be confined into planar geometry and create a monolayer to study ordering and glassy behavior of the q2D ellipsoid systems.[12,13]

In this paper we examine the orientational ordering properties of q2D hard ellipsoid systems, where particles are allowed to rotate out from the confining plane to some extent, while it is assumed in first approximation that the centers of the particles are always in the same plane. Switching on the out-of-plane orientational freedom by a gradual increase (decrease) of the limiting polar angle (θ_c) for oblate (prolate) shapes, it is possible to make a link between strictly 2D hard ellipse (hard disk) systems for prolate (oblate) shapes and q2D freely rotating prolate (oblate) ellipsoid systems. We show that the additional out-of-plane orientational freedom changes substantially the orientational ordering and the transition properties of both oblate and prolate shaped ellipsoids. To maximize the available free area on the confining surface, the axis of revolution of the prolate particle leans out from the plane, while the oblate particle leans into the plane. As a consequence, the freely rotating prolate ellipsoids resemble hard disks at high densities, while those of oblate ellipsoids behave similarly to hard ellipses. The isotropic–nematic phase transition of hard ellipses corresponds to a planar nematic–biaxial nematic phase transition of the oblate ellipsoids. Here we note that our present work can be considered as an extension of our previous studies done for monolayers of uniaxial and biaxial hard particles using restricted-orientation approximation and simulations.[35,39,40]

The paper is organized as follows. The molecular model and the details of the confinement are presented in Section II. Section III is devoted to the Parsons–Lee theory of q2D hard ellipsoid fluids, where we show how to determine the equilibrium free energy, surface coverage (2D packing fraction), and order parameters of the uniaxial and biaxial nematic phases. Technical details of the replica exchange Monte Carlo simulation method are given in Section IV. The ordering properties, the equation of state and the phase diagram of confined hard ellipsoids are presented in Section V. Finally, some conclusions are drawn in Section VI.

II. Molecular model

In this work we examine the q2D system of hard ellipsoids, where the particles are allowed to rotate freely in a restricted region of the solid angle, while the centers of particles can move only on a two-dimensional XY plane. The shape of the particles can be both prolate and oblate, *i.e.* the aspect ratio or shape anisotropy ($\kappa = \sigma_\parallel/\sigma_\perp$, where $\sigma_\parallel$ and $\sigma_\perp$ are the lengths along and perpendicular to the axis of revolution of the ellipsoid, respectively) can be either larger than one ($\kappa > 1$, prolate shape) or between zero and one ($0 < \kappa < 1$, oblate shape). The orientational restriction takes place only in the polar angle (θ), which is measured from the axis of revolution of each particle to the normal of the confining XY plane. While the particles can rotate freely in the azimuthal angle ($0 < \varphi < 2\pi$), the allowed
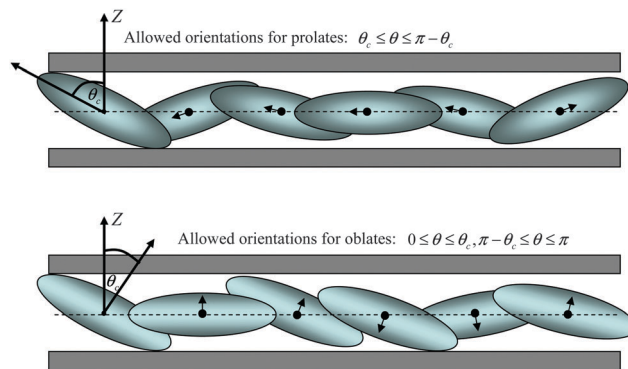

Fig. 1 Schematic representation of the system of confined hard ellipsoids: prolate ellipsoids (upper panel) and oblate ellipsoids (lower panel). The particles are confined both positionally and orientationally. The centre of mass of the ellipsoid is always in the XY plane, which is denoted by the dashed line, while the ellipsoid can rotate freely in the azimuthal angle (φ) and is restricted by the polar angle (θ_c). The arrows indicate the direction of the main symmetry axis of the ellipsoids.

range of the polar angle is different for prolate and oblate ellipsoids, namely, the range of the polar angle is given by $\theta_c < \theta < \pi - \theta_c$ for prolate shapes, while $0 < \theta < \theta_c$ and $\pi - \theta_c < \theta < \pi$ intervals are allowed for oblate ones (see Fig. 1). We can tune θ_c between 0 and $\pi/2$. In the case of prolate ellipsoids ($\kappa > 1$) $\theta_c = 0$ corresponds to the confined system of freely rotating particles, while $\theta_c = \pi/2$ gives the two-dimensional system of hard ellipses. The situation is different for oblate ellipsoids ($0 < \kappa < 1$), because the hard disk limit is given by $\theta_c = 0$, while the freely rotating system of confined oblate ellipsoids corresponds to $\theta_c = \pi/2$. The interaction between ellipsoids is purely hard, *i.e.* the pair potential between two particles is given by

$$u(r_{12}, \vec{\omega}_{12}, \vec{\omega}_1, \vec{\omega}_2) = \begin{cases} \infty & \text{for } r_{12} \leq \sigma(\vec{\omega}_{12}, \vec{\omega}_1, \vec{\omega}_2) \\ 0 & \text{otherwise} \end{cases}, \quad (1)$$

where r_{12} is the centre-to-centre distance, $\vec{\omega}_{12} = (\cos\varphi_{12}, \sin\varphi_{12}, 0)$ is the unit vector connecting the centers of the two ellipsoids, $\vec{\omega}_i = (\sin\theta_i\cos\varphi_i, \sin\theta_i\sin\varphi_i, \sin\varphi_i, \cos\theta_i)$ is the orientational unit vector of particle i ($i = 1, 2$) and $\sigma(\cdots)$ is the distance of the closest approach. Note that the third component of $\vec{\omega}_{12}$ is always zero, which ensures that the centers of the particles are always in the XY plane. The distance of the closest approach between two ellipsoids ($\sigma(\cdots)$) is approximated in the manner proposed in our previous reports.[41,42]

III. Parsons–Lee theory

To describe theoretically the orientational ordering properties of the monolayer of hard ellipsoids we derive our working equations from the well-known Parsons–Lee (PL) theory of hard bodies,[43,44] which proved to be very successful in the determination of the equation of state and the transition properties of isotropic–nematic (I–N) phase coexistence of non-spherical hard body fluids both in two[23,24] and three dimensions.[45–47] Here we present only the important ingredients of the theory,

specific equations for the ellipsoid monolayer and some technical details.

It is customary to deal with the free energy of the system, which is the sum of ideal and excess free energy terms, *i.e.* $F = F_{id} + F_{ex}$. The ideal term can be determined exactly from

$$\frac{\beta F_{id}}{N} = \log \rho - 1 + \int d\omega f(\omega) \ln(f(\omega)), \qquad (2)$$

where $\beta = 1/k_B T$ is the inverse temperature, N is the number of particles, $\rho = N/A$, A is the area of the plane, $\omega = (\varphi, \theta)$ is the collection azimuthal and polar angles, $d\omega = d\varphi\, d\theta \sin\theta$ and $f(\omega)$ is the normalized orientational distribution function $\left(\int d\omega f(\omega) = 1\right)$. The ranges of the azimuthal and polar angles in the integrals have been already given in Section II. The excess free energy contribution can be obtained approximately with the mapping procedure from the actual system to a reference one, where the second virial coefficient and the excess free energy can be obtained with good accuracy. In our case we choose the system of 2D hard disks as a reference system, because our confined ellipsoid system is q2D. The second virial coefficient of the hard disks is given by $B_2^{HD} = D^2\pi/2$, where D is the diameter of the hard disk. A luckily simple and accurate expression can be derived for the excess free energy of hard disks, too, using the scaled particle theory[48]

$$\frac{\beta F_{ex}^{HD}}{N} = -\ln(1 - \eta_{HD}) + \frac{\eta_{HD}}{1 - \eta_{HD}}, \qquad (3)$$

where $\eta_{HD} = \rho a_{HD}$ is the packing fraction of the hard disk and $a_{HD} = B_2^{HD}/2$ is the area of the hard disk. To perform the mapping procedure from the hard ellipsoids into hard disks we introduce the surface coverage (or 2D packing fraction) of the hard ellipsoids, because the intersection of the ellipsoid with the *XY* plane is an ellipse with characteristic lengths depending on the orientation of the ellipsoid. These characteristic lengths of the ellipse can be calculated easily using simple geometry. One can derive that $\sigma_{\perp,e} = \sigma_\perp$ and $\sigma_{\parallel,e} = \sigma_\parallel \sigma_\perp \big/ \sqrt{\sigma_\perp^2 \sin^2\theta + \sigma_\parallel^2 \cos^2\theta}$, where θ is the polar angle of the ellipsoid. This means that the monolayer of the hard ellipsoids can be visualized as a multi-component mixture of hard ellipses on the *XY* plane. Using the dimensions of the hard ellipse, the intersected area of the hard ellipsoid with the *XY* plane can be obtained from

$$a(\theta) = \frac{\pi \sigma_\perp^2 \sigma_\parallel}{4\sqrt{\sigma_\perp^2 \sin^2\theta + \sigma_\parallel^2 \cos^2\theta}}. \qquad (4)$$

This polar angle dependent area together with the orientational distribution function allows us to determine the surface coverage of the plane by ellipses, which is given by $\eta = \rho\langle a\rangle$, where the average area of the intersected ellipse can be determined from $\langle a\rangle = \int d\omega a(\theta) f(\omega)$. Note that the surface coverage gives back the packing fraction of hard disks in the hard-sphere limit, because $\sigma_\parallel = \sigma_\perp = D$ and the distribution function is a constant. In the PL approach the area of hard disks and the average area of hard ellipses are assumed to be the same ($a_{HD} = \langle a\rangle$), which implies also that $\eta_{HD} = \eta$ due to one-to-one

correspondence between the two systems. Based on the concept of Parsons and Lee we can now calculate the excess free energy of the monolayer of hard ellipsoids using the thermodynamic properties of hard disks as follows

$$\frac{\beta F_{ex}}{N} \approx \frac{\beta F_{ex}^{HD}}{N} \frac{B_2^{HE}}{B_2^{HD}}, \qquad (5)$$

where the second virial coefficient of hard ellipsoids restricted to the *XY* plane is given by

$$B_2^{HE} = \frac{1}{2}\int d\omega_1 f(\omega_1) \int d\omega_2 f(\omega_2) A_{exc}(\omega_1, \omega_2) \qquad (6)$$

This equation contains the excluded area between two ellipsoids, which can be obtained from the distance of the closest approach (σ) as follows

$$A_{exc}(\omega_1, \omega_2) = \frac{1}{2}\int_0^{2\pi} d\varphi_{12} \sigma^2(\omega_1, \omega_2, \omega_{12}). \qquad (7)$$

Using eqn (3)–(6) and $\eta_{HD} = \eta$ condition the excess free energy of the system becomes

$$\frac{\beta F_{ex}}{N} = \left(-\ln(1 - \eta) + \frac{\eta}{1 - \eta}\right) \frac{\int d\omega_1 f(\omega_1)\int d\omega_2 f(\omega_2) A_{exc}(\omega_1, \omega_2)}{4\int d\omega a(\theta) f(\omega)}. \qquad (8)$$

The sum of eqn (2) and (8) constitutes our density functional equation to determine the equilibrium orientational distribution function ($f(\omega)$) and the total free energy density at a given density ($\rho = N/A$). The minimization of the free energy functional with respect to $f(\omega)$ gives the Euler–Lagrange equation for the equilibrium $f(\omega)$. Note that the minimization must be carried out by maintaining the normalization condition $\left(\int d\omega f(\omega) = 1\right)$. Although the minimization procedure is very simple and straightforward, we do not present the equation of $f(\omega)$, since the resulting equation is too long. Once the equilibrium $f(\omega)$ is determined with a standard iterative method, the free energy density can be obtained by the substitution of the resulting $f(\omega)$ into the free energy functional (sum of eqn (2) and (8)). We determine the pressure from the free energy using $P = \rho^2 \partial(F/N)/\partial\rho$ and examine the orientational ordering properties of the monolayer by the standard uniaxial and biaxial order parameters. These are defined as

$$S = \langle P_2\rangle = \int d\omega f(\omega) P_2(\cos\theta), \qquad (9)$$

and

$$\Delta = \int d\omega f(\omega) \sin^2\theta \cos(2\varphi), \qquad (10)$$

where $P_2(x) = 3x^2/2 - 1/2$ is the second order Legendre polynomial. The uniaxial order parameter (S) is positive for out-of-plane ordering ($0 < S < 1$), while it is negative for in-plane ordering ($-1/2 < S < 0$). The biaxial order parameter (Δ) can be very useful in finding in-plane orientational ordering transitions, because Δ is zero for in-plane complete disorder, while it is nonzero for in-plane order. S is practically a three-dimensional order parameter of bulk ellipsoids, while Δ is the corresponding two-dimensional one of bulk ellipses

when $\theta = \pi/2$. Since our system is q2D, we need both of them. To see the effect of out-of-plane orientational freedom and to which extent the particles are tilted off from the confining plane, we determine the average aspect ratio of the effective ellipse system, which is defined as $k_{\text{eff}} = \langle \sigma_{\parallel,e}/\sigma_{\perp,e} \rangle$. In Section V we present the density and the pressure in dimensionless units, which are defined as $\rho^* = \dfrac{N}{A}\sigma_\perp^2$ and $P^* = \beta P \sigma_\perp^2$.

IV. Replica exchange Monte Carlo simulation

As for the 2D hard ellipse study,[35] we are implementing the replica exchange Monte Carlo technique.[49–51] This is done to avoid, as far as possible, the inherent hysteresis associated with transitions.[52] This method is based on the definition of an extended ensemble with partition function $Q_{\text{ext}} = \prod\limits_{i=1}^{n_r} Q_i$, where Q_i is the partition function of ensemble i. n_r ensembles are considered, and n_r replicas are employed to sample the extended ensemble, each one at each ensemble. Defining Q_{ext} allows introducing swap trial moves between any two replicas, whenever the detailed balance condition is satisfied. In our case it is convenient to expand isobaric–isothermal ensembles in pressure.[53] This is so since we are studying hard particles. Hence, the partition function of the extended ensemble reads[53,54]

$$Q_{\text{ext}} = \prod_{i=1}^{n_r} Q_{NTP_i}, \tag{11}$$

where Q_{NTPi} is the partition function of the isobaric–isothermal ensemble of the system at pressure P_i and temperature T. N particles are taken into account at each ensemble. A standard implementation is used to sample the NTP_i ensembles. This implies independent trial 2D displacements, 3D rotations of single ellipsoids, and area changes of the simulation cell. In the case of having confining planes, 3D rotations of single ellipsoids are constrained by their presence. We are also accounting for non-orthogonal parallelogram cells and so, additional trial changes of the angles and relative length sides of the cell lattice vectors are included. The following acceptance rule is set[53]

$$P_{\text{rm,acc}} = \min(1, \exp\{\beta(P_i - P_j)(A_i - A_j)\}) \tag{12}$$

where $A_i - A_j$ is the area difference between replicas i and j. Adjacent pressures must be close to provide swap acceptance rates over 0.1. Simulations are started from a packed triangular arrangement of spheres which are elongated in the direction normal to the plane by a factor κ. In the case of oblates, a stretching factor κ is also applied in a certain in-plane direction. Conversely to the stretching of spheres in a 3D cell, this procedure leads to the largest packed arrangement of spheroids in a plane.[55] A stationary state is reached faster by decompressing packed cells than by compressing lose random configurations.[52] We perform the necessary trial moves to observe a stationary state. At this stage we adjust maximum displacements to produce acceptance rates close to 0.3. We also relocate all pressures,

initially set by following a geometric progression with the replica index, to obtain similar swap acceptance rates for all pairs of adjacent ensembles. Next, we perform 4×10^{12} sampling trials for fixed maximum particle displacements, maximum rotational displacements, maximum area changes, and maximum changes of the lattice vectors. Verlet neighbor lists[56] are used to improve performance. We set $N \sim 400$ ellipsoids and n_r as a function of the pressure range to be covered. $N \sim 400$ is sufficiently large to access the properties we are showing in this study in view of Xu *et al.* analysis of system size effects.[33] However, much larger system sizes are needed to precisely determine the nature of transitions.[57] More details on the employed methods are given in our previous work.[52]

V. Results and discussion

In this section we present our theoretical and simulation results for hard ellipses, orientationally restricted and freely rotating monolayers of hard ellipsoids. The equation of state, the surface coverage, the in-plane (Δ) and out-of-plane (S) order parameters and the I–N transition densities are determined for various values of shape anisotropy. We start with the system of hard ellipses, which is obtained by setting the polar angles of all ellipsoidal particles (θ) to be $\pi/2$. This condition is accompanied by $f(\omega) = f(\varphi)$ and that the uniaxial order parameter (S) is always $-1/2$ and the biaxial order parameter can be obtained from $\Delta = \int_0^{2\pi} \mathrm{d}\varphi f(\varphi) \cos(2\varphi)$. Note that Δ now serves as a 2D orientational order parameter. The theoretical calculations and simulations can also be carried out with both oblate-shaped ($0 < \kappa < 1$) and prolate-shaped hard ellipsoids ($\kappa > 1$), where $\theta = \pi/2$ for all particles. Here we perform the hard ellipse study using oblate-shaped ellipsoids. Fig. 2 shows the pressure and the 2D order parameter (Δ) as a function of density for $\kappa^{-1} = 3$, 4, 5, 10 and 20. One can see that more particles on the surface (higher densities) are required to maintain the same value of the pressure with increasing shape anisotropy. This is due to the fact that the XY plane becomes more spacious with increasing κ^{-1}, as $\sigma_\parallel$ must be decreased at fixed $\sigma_\perp$. It can also be seen in Fig. 2 that the simulation data are well reproduced by the approximate PL theory except the values of the order parameters of the N phases corresponding to extremely anisotropic particles ($\kappa^{-1} = 10$ and 20). These data well agree with those given in ref. 33. The order parameter curves reveal for the occurrence of an isotropic–nematic phase transition, because the phase is isotropic at low densities ($\Delta = 0$), while it is nematic at high ones ($\Delta > 0$). The phase transition is of second order in the theory, while the histograms built from simulations in the vicinity of the phase transition suggest a continuous transition (probably a Kosterlitz–Thouless type). Both the theory and the simulation show the same tendencies for I–N transition densities and packing fractions (see Fig. 3). Making the ellipsoids more anisotropic one can see that the I–N transition density increases, while the I–N packing fraction decreases. This apparent contradiction is due to the fact that the increasing shape anisotropy makes the system more spacious ($\sigma_\perp$ is constant, while $\sigma_\parallel$ is decreasing),
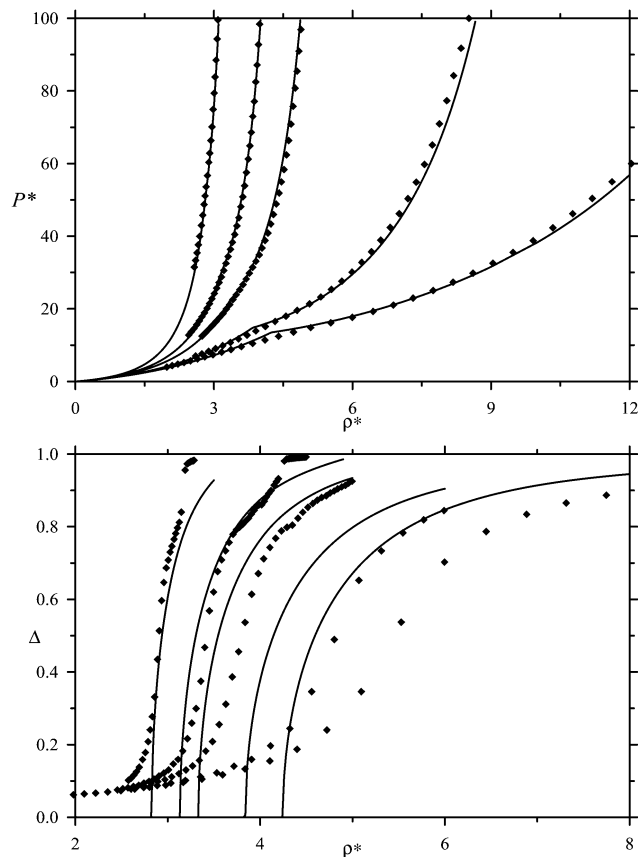
Fig. 2 Orientational ordering of the system of hard ellipses: the equation of state (upper panel) and the two-dimensional order parameter *vs.* density (lower panel). The curves correspond to κ^{-1} = 3, 4, 5, 10 and 20 from left to right. The curves are the results of PL theory, while the diamond symbols correspond to MC simulation results. The hard ellipse system is obtained from oblate ellipsoids by tilting their orientations into the *XY* plane.
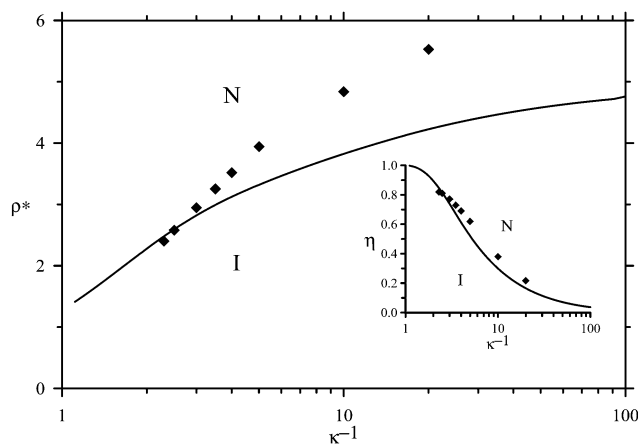

Fig. 3 Shape dependence of the isotropic–nematic (I–N) transition of hard ellipses: reduced density *vs.* aspect ratio. The curves are the results of PL theory, while the diamond symbols correspond to MC simulation results. The inset shows the packing fraction of the I–N transition as a function of aspect ratio, where $\eta = \rho \pi \sigma_{\parallel} \sigma_{\perp}/4$.

which requires more particles for the initiation of the phase transition, while the *XY* plane can be less occupied at the

same time. It can also be seen that the theory underestimates the I–N transition densities and packing fractions to a higher extent with increasing shape anisotropy, which is due to the fact that the contribution of higher order virial coefficients is not negligible with increasing κ^{-1}.

The monolayer of freely rotating hard ellipsoids can be achieved by using $\theta_c = \pi/2$ and $\theta_c = 0$ limiting angles for oblate and prolate shapes, respectively. The resulting surface coverage (2D packing fraction), effective aspect ratio, pressure and order parameters are shown for prolate and oblate shaped ellipsoids in Fig. 4 and 5, respectively. The effective aspect ratio of the corresponding hard ellipse system is given by $\kappa_{\mathrm{eff}} = \langle \sigma_{\parallel,e}/\sigma_{\perp,e} \rangle = \langle \kappa / \sqrt{\sin^2\theta + \kappa^2\cos^2\theta} \rangle$, which is the average aspect ratio of the ellipses obtained by intersecting the ellipsoids with the *XY* plane. In turn, the surface coverage can be obtained with the help of κ_{eff} as follows: $\eta = \rho^*\pi\kappa_{\mathrm{eff}}/4$. Starting with prolate ellipsoids, one can see that the particles do not form an isotropic phase ($S > 0$), but they align along the normal of the *XY* plane (see the simulation snapshot of Fig. 4)
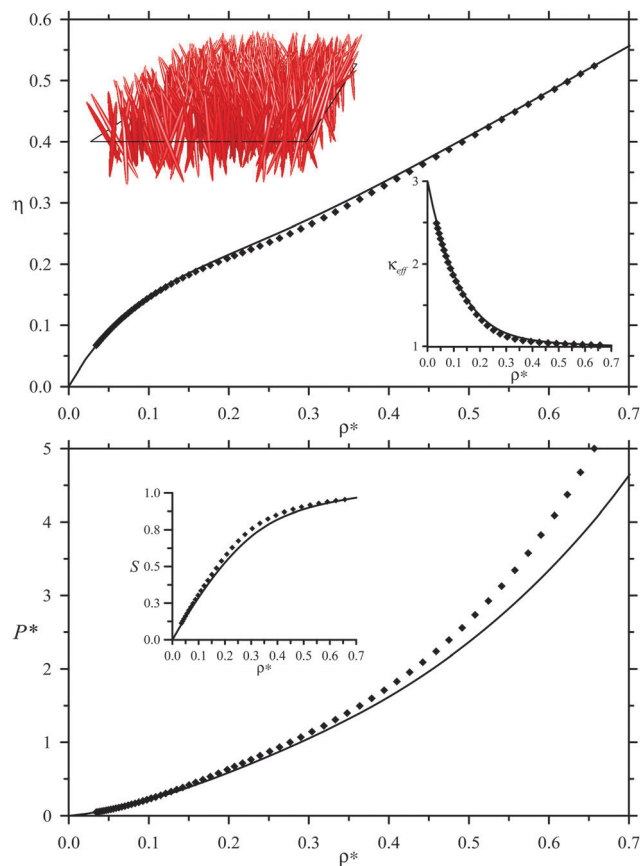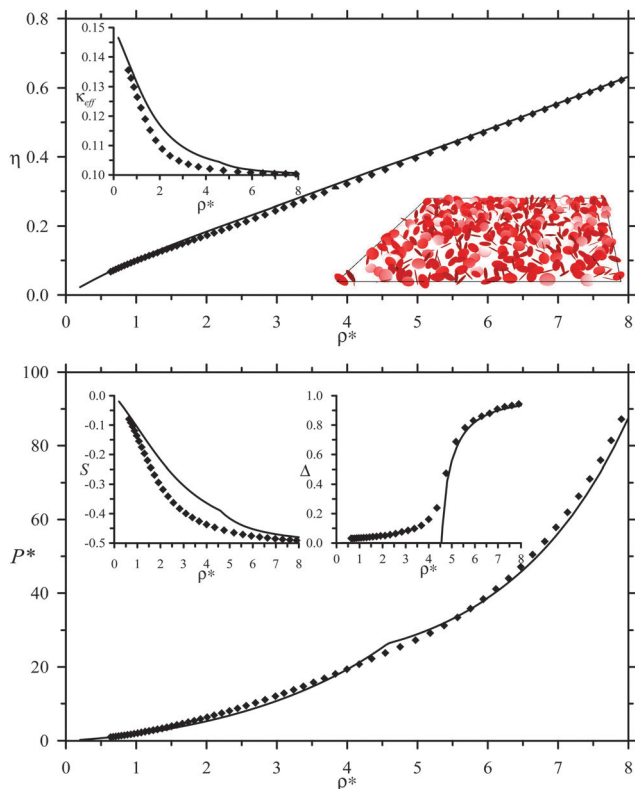

Fig. 4 Monolayer of freely rotating hard prolate ellipsoids: surface coverage (packing fraction) *vs.* reduced density (upper panel) and the equation of state (lower panel) at $\kappa = 10$. The effective aspect ratio of the corresponding hard ellipse system $\left(\kappa_{\mathrm{eff}} = \langle \sigma_{\parallel,e}/\sigma_{\perp,e} \rangle = \langle \kappa / \sqrt{\sin^2\theta + \kappa^2\cos^2\theta} \rangle\right)$ is shown in the inset of the upper panel, while the out-of-plane order parameter (S) is presented in the inset of the lower panel. The curves are the results of PL theory, while the diamond symbols correspond to MC simulation results. The snapshot is the result of replica exchange Monte Carlo simulation method.
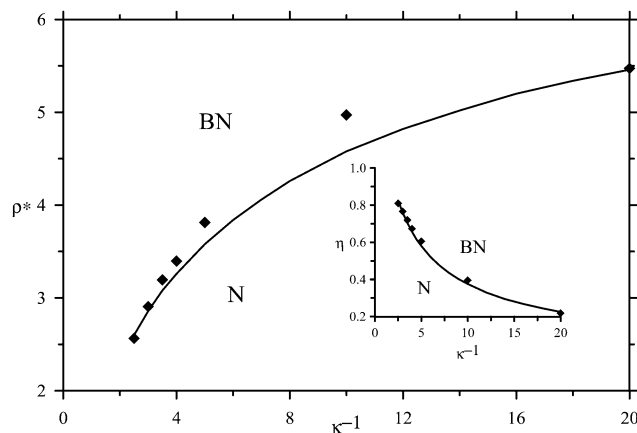
Fig. 5 Monolayer of freely rotating hard oblate ellipsoids: surface coverage (packing fraction) *vs.* reduced density (upper panel) and the equation of state (lower panel) at $\kappa = 1/10$. The effective aspect ratio of the corresponding hard ellipse is shown in the inset of the upper panel, while the out-of-plane (S) and the in-plane (Δ) order parameters are presented in the inset of the lower panel. The curves are the results of PL theory, while the diamond symbols correspond to MC simulation results. The snapshot is the result of the replica exchange Monte Carlo simulation method.

even at very low densities. In fact, an isotropic phase would appear only at the limit of infinite dilution, where S converges to zero (see the inset of Fig. 4). The reason for this is that some configurations are always present with distances between neighboring particles less than $\sigma_\parallel$. These configurations contribute with positive values to the order parameter. The density dependence of the surface coverage and the effective aspect ratio show that the particles have less and less chance to lie into the *XY* surface with increasing density because of packing effects. The intersection of the ellipsoid with the *XY* surface is practically a hard disk for $\rho^\star > 0.6$, where the effective ellipse aspect ratio is almost one. This makes the monolayer of hard ellipsoids very similar to the system of hard disks at high densities despite the presence of orientational fluctuations. The in-plane order parameter (eqn (10)) is always zero, while the out-of-plane order parameter (eqn (9)) is positive. This shows that the out-of-plane orientational ordering is uniaxial with the nematic director parallel to the layer normal. It can also be seen that S is very close to its maximum value ($S_{max} = 1$) at $\rho^\star > 0.7$, which corresponds to the case where all prolate ellipsoids are parallel and align along the layer normal. The reason why prolate ellipsoids prefer the out-of-plane ordering is that they can

maximize the free area available on the surface with the penalty of orientational entropy loss. Moreover the close packing structure of prolate ellipsoids is identical to that of 2D hard disks. One can also see that the theory reproduces quite well the simulation data for all properties except the equation of state at high densities.

The principle of minimizing the intersected area with the *XY* plane applies also for oblate ellipsoids (see Fig. 5). The minimal intersected area, which is actually an ellipse with $\sigma_{\parallel,e} = \sigma_\parallel$ and $\sigma_{\perp,e} = \sigma_\perp$ dimensions, can be achieved with ordering into the *XY* plane, while the out-plane ordering results in a higher intersected area, because $\sigma_\parallel < \sigma_\perp$ for oblate ellipsoids. The resulting in-plane ordering can be seen in the simulation snapshot and from the high density behavior of the effective aspect ratio ($\kappa_{eff} \rightarrow \kappa = \sigma_\parallel/\sigma_\perp$). The out of plane order parameter goes to $-1/2$, which corresponds to complete in-plane ordering. Moreover, the in-plane order is isotropic at low densities ($\Delta = 0$), while it is nematic at high densities ($\Delta > 0$). This means that the system undergoes a phase transition from a planar uniaxial nematic order ($S < 0$, $\Delta = 0$) to a biaxial nematic one ($S < 0$, $\Delta \neq 0$), which can be considered as a 2D I–N phase transition. The order of the uniaxial nematic–biaxial nematic (N–BN) phase transition is proved to be second order in the approximate PL theory, while the transition is of higher order and continuous in the simulation. This transition is the result of the competition between in-plane orientational entropy (favoring disorder) and the in-plane packing entropy (favoring order). The high density structure of the hard ellipsoid monolayer resembles the nematic phase of the 2D hard ellipses, while at low densities the structure more or less corresponds to an isotropic phase of a polydisperse mixture of hard ellipses. One can also see that the agreement between the theory and the simulation is quite good for oblate ellipsoids, which is especially true for the equation of state. An interesting feature is that the theory overestimates the out-of-plane ordering. This could stem from the effect of higher virial coefficients, which are not included in the theory. Fig. 6 shows

Fig. 6 Shape dependence of the uniaxial nematic–biaxial nematic (N–BN) transition of freely rotating hard oblate monolayer: reduced density *vs.* aspect ratio. The curves are the results of PL theory, while the diamond symbols correspond to MC simulation results. The inset shows the packing fraction of the N–BN transition as a function of aspect ratio.
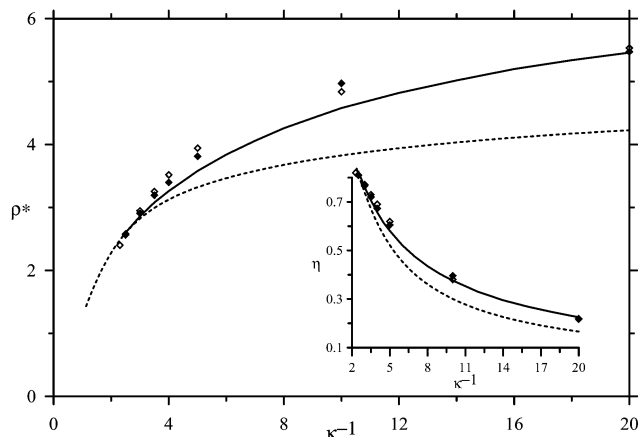
Fig. 7 Comparison of the transition densities of freely rotating hard ellipses and confined hard oblates in the reduced density–aspect ratio plane. The continuous (ellipsoids) and dashed (ellipses) curves are the results of PL theory, while the open and filled diamond symbols correspond to MC simulation results for hard ellipses and hard ellipsoids, respectively. The inset shows the packing fractions of I–N and N–BN transitions as a function of the aspect ratio.

the in-plane isotropic–nematic (or N–BN) transition densities as a function of aspect ratio resulting from the PL theory and simulation. One can see that the N–NB transition density increases with increasing shape anisotropy, while the packing fraction decreases. This is due to the fact that we go to the "volumeless" hard needle limit with decreasing κ, where the transition density saturates at a finite value, while the packing fraction vanishes (note that $\kappa_{\text{eff}} \rightarrow 0$ and $\eta = \rho^* \frac{\pi}{4} \kappa_{\text{eff}}$). The agreement for the transition densities is again very good between the theory and simulation. To see the effect of out-of-plane orientational freedom it is worth plotting the I–N densities of the 2D hard ellipse system and those of the freely rotating hard oblate monolayer together (see Fig. 7). It can be seen that the simulation does not show a substantial difference between the two systems, while the theory predicts that the out-of-plane freedom destabilizes the nematic order, *i.e.* the I–N density curve is shifted into the direction of higher densities. In the simulation the nematic phase evolves from a very ordered planar phase (isotropic in the *XY* plane), where the effective aspect ratio is almost identical with the aspect ratio of the ellipsoids (see Fig. 5), *i.e.* the corresponding hard ellipse system is almost monodisperse. This is not the case in the theory, where the transition occurs at such densities, where the corresponding hard ellipse system is still polydisperse with a larger aspect ratio (κ_{eff}) than κ. As a result the effect of out-of-plane orientational freedom is more pronounced in the theory than in the simulation. This shows that the theory exaggerates the effect of out-of-plane orientational freedom on the N–BN phase transition.

Now we show how the I–N transition properties change with switching on the out of plane orientational freedom through the varying limiting polar angle (θ_c), which is between 0 and $\pi/2$ for both prolate and oblate shapes. If $\theta_c = \pi/2$ ($\cos \theta_c = 0$) the prolate ellipsoids on the *XY* plane behave like the system of
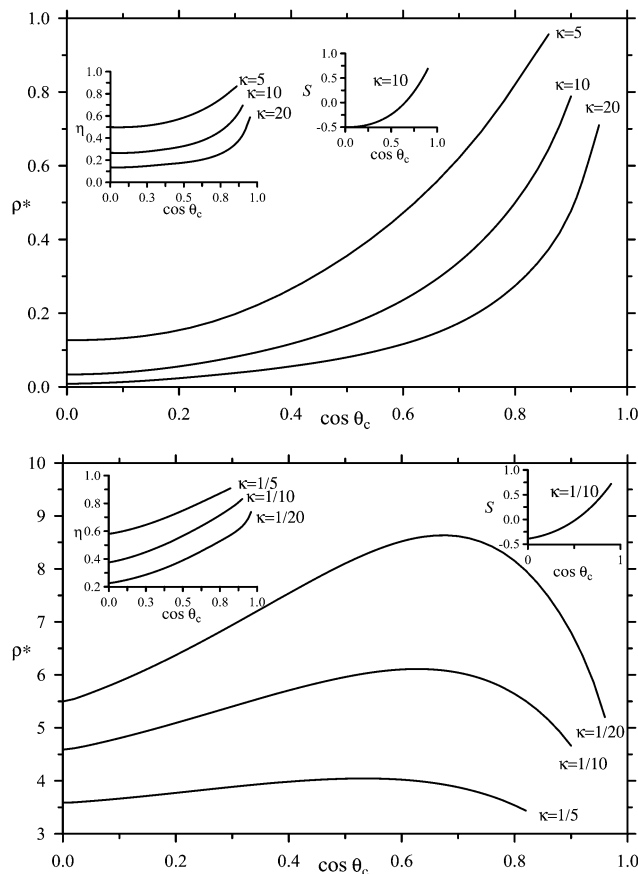

Fig. 8 Monolayers of orientationally restricted hard ellipsoids: uniaxial nematic–biaxial nematic (N–BN) transition density *vs.* $\cos \theta_c$. The upper panel is for prolate shapes while the lower one for oblate shapes. Insets show the $\cos \theta_c$ dependence of the surface coverage and the out-of-plane order parameter at the N–BN ordering transition. The curves are the results of PL theory.

hard ellipses, *i.e.* they undergo a 2D I–N phase transition with increasing density (see Fig. 8). However this phase transition is destabilized with decreasing the limiting angle (θ_c), which corresponds to increasing $\cos \theta_c$. As the orientational window is widened (decreasing θ_c), the prolate ellipsoids tend to minimize their occupied area on the *XY* surface, which results in less anisotropic in-plane ellipses and higher transition densities for all studied aspect ratios. In addition to this, the in-plane order transforms continuously into the out-of-plane order, *i.e.* S becomes positive with $\cos \theta_c$ (see the inset of Fig. 8). Hence, the 2D I–N transitions turn into N–BN transitions for confined prolates which are lost for the free rotating case. The surface coverage curves show very clearly that the occupied area on the *XY* surface increases enormously upon decreasing the polar angle restriction at the transition, *i.e.* the 2D I–N phase transition is destabilized with decreasing θ_c. The value of θ_c where the orientational ordering transition is preempted by the positional one (freezing transition) cannot be determined with the present PL theory. Interestingly, MC simulation shows that the I–N density is practically not affected by the value of limiting polar angle, but the transition disappears at values of θ_c close to zero.

Note that the I–N transition density and surface coverage curves move into the direction of lower densities with increasing shape anisotropy because the occupied area of the ellipsoids becomes larger with increasing κ as $\sigma_{\parallel} > \sigma_{\perp}$. The case of oblate ellipsoids is different because $\theta_c = \pi/2$ corresponds to the freely rotating limit, while $\theta_c = 0$ is the hard disk limit. Starting from the freely rotating case one can see that the I–N transition density shows a maximum at an intermediate value of θ_c, which can be attributed to the combined effect of decreasing in-plane shape anisotropy and the increasing intersected area of the ellipsoids with decreasing θ_c. The N–BN transition packing fraction behaves simply since it is always an increasing function of $\cos\theta_c$, *i.e.* the nematic phase is destabilized with stronger orientational restriction. This means that the N–NB curve and the nematic-solid curves must cross each other at a threshold value of $\cos\theta_c$ making the biaxial nematic order metastable and producing a plastic solid (an orientationally disordered solid). This plastic solid would eventually turn into an orientationally ordered solid at higher densities. Finally, the S order parameter shows that the system undergoes a structural change from the in-plane order into the out-of-plane order with a narrowing orientational window.

Finally, it is interesting to compare the global phase diagram of freely rotating ellipsoids with that of 2D hard ellipses,[35] which are shown together in Fig. 9. To build the global phase diagram, which includes plastic and oriented solid phases too, we have followed the procedure given in ref. 35. This involves determining the frequency-density histograms, the compressibility from density fluctuations and the appropriate global order parameters to detect the transitions between differently ordered phases. These functions give, in addition, some hints on the nature of the phase transitions. The way a 2D solid melts into fluid involves a subtle continuous transition to produce a hexatic phase first, which then undergoes a first order transition to yield the fluid.[57] All these happen in a relatively small packing fraction window. The hexatic phase is

characterized by quasi-long-range bond orientational correlations instead of the preserved long range bond orientational correlations of the solid phase (the 2D solid phase does not preserve positional correlations, though).[58,59] Thus, a precise determination of the hexatic boundaries requires long-scale computer simulations.[57] This is out of the scope of this work and we are not including the hexatic phase in Fig. 9. The hexatic phase is located somewhere between the solid and the fluid phases where we are simply reporting a solid–fluid coexistence. In this figure, one can see that the phase diagram of freely rotating oblate ellipsoids is similar to that of 2D ellipses when considering the effect of the out-of-plane orientational freedom. This supports the idea that the 2D hard ellipse system can be considered as a fairly good approximation of the freely rotating ellipsoids, because the uniaxial nematic, biaxial nematic and solid phases of oblates correspond to the isotropic, nematic and solid phases of 2D ellipses. One can also see that the prolate ellipsoids undergo a nematic–plastic solid phase transition similar to the freezing of 2D hard disks, *i.e.* the observed uniaxial nematic and plastic solid phases can be identified with the fluid and solid phases of the hard disks. The reason why we are labeling as "plastic" the prolate solid phase is that it shows uniaxial orientational ordering only and the projections of the symmetry axes on the plane are not aligned (resembling a 2D plastic phase). However, the solid phase of oblates can be both uniaxially (plastic) and biaxially oriented in the case of weak and strong shape anisotropies, respectively. As a result, uniaxial nematic–oriented solid, biaxial nematic–oriented solid, uniaxial nematic–plastic solid and plastic solid–oriented solid phase transitions can be observed by varying the aspect ratio of the ellipsoid. Practically, the out-of-plane orientational freedom does not shift the I–N and plastic solid–oriented solid phase boundaries of the 2D ellipses. However, the fluid–solid transition of the disks and the nematic–oriented solid transition of the ellipses can be affected strongly by the out-of-plane orientational freedom as the packing fractions of the co-existing phases drop with increasing shape anisotropy. This can be seen more clearly on the prolate side of Fig. 9. The reason why the freezing takes place at lower surface coverage is that the ellipsoids can collide with their out-of-plane parts, too. For large anisotropies the effective collision diameter of an ellipsoid is bigger than that of the hard disk due to the presence of out-of-plane excluded volume interactions. The difference between the two diameters increases with making the prolate (oblate) ellipsoid more elongated (flat), while the intersected area of the ellipsoid with the XY plane does not change practically. Therefore, the increasing collision diameter and the constant intersected area produce together lower 2D packing fractions for both prolate and oblate shaped ellipsoids. The out-of-plane collisions do not practically occur for quasi-spherical ellipsoids explaining why the phase diagram of ellipsoids is very similar to that of the 2D ellipse case and almost symmetric around $\kappa = 1$.
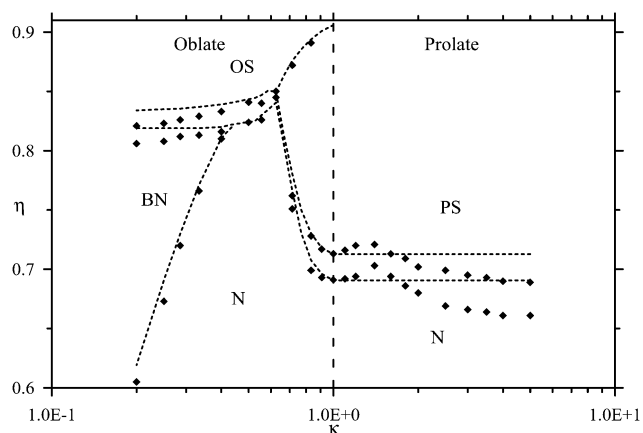

Fig. 9 Global phase diagram of freely rotating ellipsoids (diamond symbols) and that of hard ellipses (dashed curves[35]) in the packing fraction-aspect ratio plane. Labels N, BN, PS and OS denote uniaxial nematic, biaxial nematic, plastic solid and oriented solid phases, respectively. The vertical dashed line signals the spherical case and splits the chart into the oblate (left) and prolate (right) regions. The dashed curves correspond to 2D hard ellipses for $\kappa < 1$ and 2D hard disks for $\kappa > 1$.

VI. Conclusions

We have examined the orientational ordering properties of the monolayer of hard ellipsoids using the replica exchange

Monte Carlo simulation method and the Parsons–Lee density functional theory. We have found that both the shape anisotropy and the orientational restriction affect substantially the orientational order on the plane. The subtle interplay between orientational and packing entropies results in different structures and phase behaviors for prolate and oblate shaped ellipsoids. The main driving force of the ordering behavior is to minimize the intersected area between the particle and the surface to achieve the close packing structure with increasing surface density. The minimal intersected area is a disk for prolate, while it is an ellipse for oblate ellipsoids. Highly packed structures can be achieved with only out-of-plane (in-plane) ordering for prolate (oblate) ellipsoids, *i.e.* prolate ellipsoids prefer to order along the normal of the plane, while oblate ellipsoids like to order in the plane.

The monolayer of prolate ellipsoids with very small out-of-plane orientational freedom behaves almost identically to the system of 2D hard ellipses, *i.e.* it forms 2D isotropic and nematic phases. The gradual rise of the out-of-plane freedom, through decreasing θ_c, allows the ellipsoid particle to lean out from the plane and to decrease the intersected area with the confining plane. This involves less anisotropic shape in the interactions and destabilization of the biaxial nematic phase (2D nematic) with respect to uniaxial nematic one (2D isotropic). At full orientational freedom ($0 < \theta < \pi$) prolate ellipsoids do not form an isotropic phase, but they are ordered along the normal of the confining plane even at very low densities and behave similarly to the 2D system of hard disks at higher densities. The freezing transition of the freely rotating ellipsoids occurs at lower surface coverage than that of hard disks due to the presence of out of plane excluded volume interactions.

The monolayer of oblate ellipsoids without out-of-plane freedom is identical to the 2D system of hard disks. The gradually increasing freedom in the polar angle (θ) allows the oblate ellipsoid to decrease its intersected area with the confining plane through leaning out from the plane. This makes the ordering planar for the main symmetry axis of the ellipsoid. However the anisotropic interactions between the tilted ellipsoids give rise to an additional in-plane order, *i.e.* the phase is biaxial nematic, which is due to the excluded area gain coming from the in-plane ordering of elliptical intersections. In the freely rotating case the oblate ellipsoids form a planar nematic phase at low densities and a biaxial nematic one at high densities. Interestingly, the I–N density of 2D ellipses is almost identical to that of freely rotating ellipsoids confined to a plane. However, the out-of-plane excluded volume interactions shift the freezing transitions into the direction of lower surface coverage.

In summary the out-of-plane orientational freedom stabilizes the in-plane nematic ordering in the monolayer of oblate ellipsoids, while the opposite occurs in the monolayer of prolate ellipsoids. This is congruent with the 2D ellipse and 2D disk phase diagrams, which are obtained as limiting cases in this study. In our simple model we have neglected the effect of out-of-plane positional freedom which we expect to have a relatively small effect on the system behavior. On the other hand, not including a soft wall–particle interaction may lead to deviations from experimental set-ups where capillary phenomena are frequently important. No doubt, the inclusion of this interaction would substantially increase the computation burden of the problem. We leave this issue for future studies.

Acknowledgements

References

1 S. Sacanna, D. J. Pine and G.-R. Yi, *Soft Matter*, 2013, **9**, 8096.
2 W. Qi, J. de Graaf, F. Qiao, S. Marras, L. Manna and M. Dijkstra, *Nano Lett.*, 2012, **12**, 5299.
3 K. J. Lee, J. Yoon and J. Lahann, *Curr. Opin. Colloid Interface Sci.*, 2011, **16**, 195.
4 D. Florea and H. M. Wyss, *J. Colloid Interface Sci.*, 2014, **416**, 30.
5 N. F. Bouxsein, C. Leal, C. S. McAllister, K. K. Ewert, Y. Li, C. E. Samuel and C. R. Safinya, *J. Am. Chem. Soc.*, 2011, **133**, 7585.
6 R. K. Pujala, N. Joshi and H. B. Bohidar, *Colloid Polym. Sci.*, 2015, 3651, DOI: 10.1007/s00396-015-3651-3.
7 T. E. Herod and R. S. Duran, *Langmuir*, 1998, **14**, 6606.
8 F. Kim, S. Kwan, J. Akana and P. D. Yang, *J. Am. Chem. Soc.*, 2001, **123**, 4360.
9 H. Razafindralambo, A. Richel, M. Paquot, L. Lins and C. Blecker, *J. Phys. Chem. B*, 2012, **116**, 3998.
10 G. B. Davies, T. Krüger, P. V. Coveney, J. Harting and F. Bremse, *Adv. Mater.*, 2014, **26**, 6715.
11 G. B. Davies, T. Krüger, P. V. Coveney, J. Harting and F. Bremse, *Soft Matter*, 2014, **10**, 6742.
12 Z. Zheng, F. Wang and Y. Han, *Phys. Rev. Lett.*, 2011, **107**, 065702.
13 C. K. Mishra, A. Rangarajan and R. Ganapathy, *Phys. Rev. Lett.*, 2013, **110**, 188301.
14 E. L. Hansen, S. Jabbari-Farouji, H. Mauroy, T. S. Plivelic, D. Bonne and J. O. Fossuma, *Soft Matter*, 2013, **9**, 9999.
15 L. S. Li and A. P. Alivisatos, *Adv. Mater.*, 2003, **15**, 408.
16 K. Béneut, D. Constantin, P. Davidson, A. Dessombz and C. Chanéac, *Langmuir*, 2008, **24**, 8205.
17 D. Constantin, P. Davidson and C. Chanéac, *Langmuir*, 2010, **26**, 4586.
18 J. A. Cuesta and D. Frenkel, *Phys. Rev. A: At., Mol., Opt. Phys.*, 1990, **42**, 2126.
19 A. M. Somoza and R. C. Desai, *J. Phys. Chem.*, 1992, **96**, 1401.
20 D. Kramer, A. Ben-Shaul, Z.-Y. Chen and W. M. Gelbart, *J. Chem. Phys.*, 1992, **96**, 2236.
21 M. R. Fisch and C. Rosenblatt, *J. Phys. II*, 1994, **4**, 103.
22 H. Schlacken, H.-J. Mogel and P. Schiller, *Mol. Phys.*, 1998, **93**, 777.
23 S. Varga and I. Szalai, *Mol. Phys.*, 1998, **95**, 515.

24 S. Varga and I. Szalai, *J. Mol. Liq.*, 2000, **85**, 11.

25 R. van Roij, M. Dijkstra and R. Evans, *J. Chem. Phys.*, 2000, **113**, 7689.

26 R. van Roij, M. Dijkstra and R. Evans, *Europhys. Lett.*, 2000, **49**, 350.

27 A. C. D. van Enter and S. B. Shlosman, *Phys. Rev. Lett.*, 2002, **89**, 285702.

28 M. Cosentino Lagomarsino, M. Dogterom and M. Dijkstra, *J. Chem. Phys.*, 2003, **119**, 3535.

29 Y. Martínez-Ratón, E. Velasco and L. Mederos, *J. Chem. Phys.*, 2005, **122**, 064903.

30 Y. Martínez-Ratón, E. Velasco and L. Mederos, *J. Chem. Phys.*, 2006, **125**, 014501.

31 R. L. C. Vink, *Phys. Rev. Lett.*, 2007, **98**, 217801.

32 Y. Martínez-Ratón, *Liq. Cryst.*, 2011, **38**, 697.

33 W.-S. Xu, Y.-W. Li, Z.-Y. Sun and L.-J. An, *J. Chem. Phys.*, 2013, **139**, 024501.

34 R. K. Pujala and H. B. Bohidar, *Phys. Rev. E: Stat., Nonlinear, Soft Matter Phys.*, 2013, **88**, 052310.

35 G. Bautista-Carbajal and G. Odriozola, *J. Chem. Phys.*, 2014, **140**, 204502.

36 W.-S. Xu, X. Duan, Z.-Y. Sun and L.-J. An, *J. Chem. Phys.*, 2015, **142**, 224506.

37 D. Frenkel and R. Eppenga, *Phys. Rev. A: At., Mol., Opt. Phys.*, 1985, **31**, 1776.

38 Z. Zhang, P. Pfleiderer, A. B. Schofield, C. Clasen and J. Vermant, *J. Am. Chem. Soc.*, 2011, **133**, 392.

39 M. González-Pinto, Y. Martínez-Ratón, E. Velasco and S. Varga, *PCCP*, 2015, **17**, 6389.

40 Y. Martínez-Ratón, S. Varga and E. Velasco, *J. Chem. Phys.*, 2014, **140**, 204906.

41 E. Meneses-Juarez, S. Varga, P. Orea and G. Odriozola, *Soft Matter*, 2013, **9**, 5277.

42 S. Varga, E. Meneses-Juarez and G. Odriozola, *Soft Matter*, 2013, **9**, 11178.

43 J. D. Parsons, *Phys. Rev. A: At., Mol., Opt. Phys.*, 1979, **19**, 1225.

44 S. D. Lee, *J. Chem. Phys.*, 1987, **87**, 4972; S. D. Lee, *J. Chem. Phys.*, 1988, **89**, 7036.

45 S. C. McGrother, D. C. Williamson and G. Jackson, *J. Chem. Phys.*, 1996, **104**, 6755.

46 P. J. Camp, C. P. Mason, M. P. Allen, A. A. Khare and D. A. Kofke, *J. Chem. Phys.*, 1996, **105**, 2837.

47 P. Padilla and E. Velasco, *J. Chem. Phys.*, 1997, **106**, 10299.

48 H. Reiss, H. L. Frisch and J. L. Lebowitz, *J. Chem. Phys.*, 1959, **31**, 369.

49 E. Marinari and G. Parisi, *Europhys. Lett.*, 1992, **19**, 451.

50 A. P. Lyubartsev, A. A. Martinovski, S. V. Shevkunov and P. N. Vorontsov-Velyaminov, *J. Chem. Phys.*, 1992, **96**, 1776.

51 K. Hukushima and K. Nemoto, *J. Phys. Soc. Jpn.*, 1996, **65**, 1604.

52 G. Bautista-Carbajal, A. Moncho-Jordá and G. Odriozola, *J. Chem. Phys.*, 2013, **138**, 064501.

53 G. Odriozola, *J. Chem. Phys.*, 2009, **131**, 144107.

54 T. Okabe, M. Kawata, Y. Okamoto and M. Mikami, *Chem. Phys. Lett.*, 2001, **335**, 435.

55 A. Donev, F. H. Stillinger, P. M. Chaikin and S. Torquato, *Phys. Rev. Lett.*, 2004, **92**, 255506.

56 A. Donev, S. Torquato and F. H. Stillinger, *J. Comput. Phys.*, 2005, **202**, 737.

57 E. P. Bernard and W. Krauth, *Phys. Rev. Lett.*, 2011, **107**, 155704.

58 J. M. Kosterlitz and D. J. Thouless, *J. Phys. C: Solid State Phys.*, 1973, **6**, 1181.

59 B. I. Halperin and D. R. Nelson, *Phys. Rev. Lett.*, 1978, **41**, 121.